

Inferring the population properties of binary black holes from unresolved gravitational waves

Rory J. E. Smith,^{1,2} Colm Talbot,^{3,1,2} Francisco Hernandez Vivanco^{1,2}
and Eric Thrane^{1,2}

¹School of Physics and Astronomy, Monash University, Vic 3800, Australia

²OzGrav: The ARC Centre of Excellence for Gravitational Wave Discovery, Clayton VIC 3800, Australia

³LIGO, California Institute of Technology, Pasadena, CA 91125, USA

22 April 2020

ABSTRACT

The vast majority of compact binary mergers in the Universe produce gravitational waves that are too weak to yield unambiguous detections; they are unresolved. We present a method to infer the population properties of compact binaries—such as their merger rates, mass spectrum, and spin distribution—using both resolved and unresolved gravitational waves. By eliminating entirely the distinction between resolved and unresolved signals, we eliminate bias from selection effects. To demonstrate this method, we carry out a Monte Carlo study using an astrophysically motivated population of binary black holes. We show that some population properties of compact binaries are well constrained by unresolved signals after about one week of observation with Advanced LIGO at design sensitivity.

1 INTRODUCTION

Every year, around 2×10^6 binary neutron stars and 1.5×10^5 binary black holes merge somewhere in the Universe, radiating gravitational waves Abbott et al. (2018a). Only a small fraction of these signals are detected by observatories such as Advanced LIGO (aLIGO), Advanced Virgo, and KAGRA Acernese et al. (2014); Aasi et al. (2015); Akutsu et al. (2019). The rest are too faint to be resolved. Nonetheless, the ensemble of unresolved gravitational-wave signals forms an astrophysical background, which *can* be detected by advanced gravitational-wave detectors Abbott et al. (2018a, 2016b); Smith & Thrane (2018); Hernandez-Vivanco et al. (2019). Here, we use the word “background” to denote gravitational-wave signals that are not clearly detected and published in catalogs, e.g., Abbott et al. (2019). Since there are many connotations associated with the notion of a gravitational-wave background, it is worth pausing to make our meaning absolutely clear.

First, we note that this definition of “background” is detector-dependent; as gravitational-wave detectors become more sensitive, a greater fraction of binary mergers will be clearly resolved, and so what we might refer to as background now will become foreground in the future. Second, we note that the gravitational-wave background from compact binaries is often thought of as a *foreground* when looking for primordial gravitational waves from the early Universe; see, e.g., Maggiore (2000). Indeed, one scientist’s foreground is another’s background; here we use the word “foreground” to refer to resolved binaries. Finally, there is a common notion that the gravitational-wave background consists of a plethora of unimaginably faint sources. In reality, it derives from a continuum of binaries, ranging from the nearly-detectable to the clearly-not-detectable. Since there is no universally accepted definition of “detection,” the boundary between the resolved catalog and the unresolved background is fuzzy.

However one may choose to delineate this boundary, the background encodes rich information about the mass and spin distributions of compact binaries. These distributions, in turn, provide insights into binary evolution Stevenson et al. (2015, 2017); Vitale et al. (2017); Talbot & Thrane (2017a); Gerosa & Berti (2017); Farr et al. (2017); Wysocki et al. (2018); Lower et al. (2018), star formation history, the fate of massive stars Fishbach & Holz (2017); Talbot & Thrane (2018); Abbott et al. (2018a), the behavior of matter at supranuclear densities Abbott et al. (2018b), and the existence of primordial black holes Raidal et al. (2017), amongst other things. Crucially, the foreground probes only the closest binaries. By analyzing the foreground and background together, it is possible to probe the entire population of binary mergers.

Here, we use hierarchical inference¹ to extend the method outlined in Smith & Thrane (2018) in order to determine the ensemble properties of compact binaries. By eliminating the artificial distinction between foreground and background, we probe greater distances than possible with resolved events alone, while eliminating bias from selection effects. We demonstrate that it is possible to make population inferences even when excluding statistically significant, “gold-plated” detections. The key results are posterior probability distributions describing the shape of the binary black hole mass and spin distributions, derived using entirely unresolved events. We show that these posteriors are consistent with the true values used for the generation of the simulated data. We argue that this method is statistically optimal in the sense that is not possible to obtain more narrow posteriors given a fixed dataset.

This work builds on Gaebel et al. (2018), which describes how population studies can be extended to include sub-threshold candi-

¹ For a review of hierarchical inference in gravitational-wave astronomy, see Section V of Thrane & Talbot (2018).

date events, some of which are bona fide gravitational-wave signals, even though any single candidate is probably a noise fluctuation. This is part of a broader trend in gravitational-wave astronomy. For example, the arguably marginal event GW170729 was included² in the first gravitational-wave transient catalog GWTC-1 Abbott et al. (2018b) and the companion paper Abbott et al. (2018a).

We highlight a few innovations unique to this work. First, we eliminate selection effects entirely by making no distinction between detected events and sub-threshold events. Taking into account selection effects in population studies can be a somewhat subtle endeavour Thrane & Talbot (2018); Abbott et al. (2016a); Fishbach et al. (2018); Mandel et al. (2018), involving challenging efficiency calculations Ng et al. (2018); Tiwari et al. (2018). These challenges are removed by eliminating the concept of a detection threshold. Second, by eliminating the minimum detection threshold entirely, we extend the range of the analysis to include events at large redshifts, well beyond what can be probed with unambiguous detections. This is an important first step toward studying the evolution of binary populations over cosmic time, though, more work is required to measure this redshift-dependence using hyper-parameters; see Fishbach et al. (2018). Third, while Gaebel et al. (2018) generates pseudo posterior samples from a Fisher matrix approximation for the likelihood function, we calculate posterior samples using a full-fledged parameter estimation pipeline. By carrying out full parameter estimation (the main computational cost of the search), we show that our method is computationally feasible.

The remainder of this paper is organized as follows. In Section 2 we describe astrophysically motivated models of the binary black hole mass spectrum and spin distributions. In Section 3, we describe the method for population inference from a population of sub-threshold signals. In Section 4, we present the results of our Monte Carlo study. Concluding remarks are provided in Section 6.

2 POPULATION MODEL

We parameterize the mass and spin distributions using one of the prescriptions from Abbott et al. (2018a). In this section, we briefly summarize our population model. The reader is referred to the appendix for more details. Our models take the form of conditional priors $\pi_\theta(\theta|\Lambda)$ where θ are binary black hole parameters and Λ are hyper-parameters governing the shape of the θ distribution. A list of hyper-parameters, their meaning, and injection values used in this study is provided in Tab. 1.

We model the black hole mass spectrum following Talbot & Thrane (2018). The distribution is a mixture model of a truncated power-law and a Gaussian. An example of the source-frame primary mass distribution is shown in orange in Fig. 1 and the lab-frame distribution (distorted by cosmological redshift) is shown in blue. We model the distribution of black hole spin magnitudes following Wysocki et al. (2018). The distribution is a beta distribution. We model the distribution of black hole spin orientations following Talbot & Thrane (2017b). The distribution is a mixture model of an isotropic distribution and model with a preference for aligned spin. For this study, we choose a set of plausible population parameters based on Abbott et al. (2018a).

We assume a fixed, known redshift distribution of (or equivalently, luminosity distance). We assume that sources are uniformly

² The event GW170729 has an astrophysical probability ranging from $p_{\text{astro}} = 48 - 98\%$.

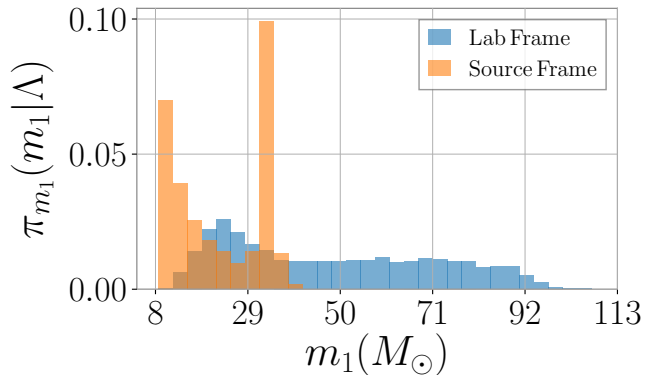


Figure 1. Astrophysically motivated primary mass (m_1) distribution in the source frame (orange) and lab frame (blue). The lab-frame mass distribution appears redshifted due to the expansion of the universe.

distributed in co-moving volume to a maximum luminosity distance of $d_L^{\max} \approx 5$ Gpc (redshift $z = 0.8$). Throughout, we assume the standard Λ CDM cosmology ($\Omega_\Lambda = 0.69, \Omega_m = 0.31, H_0 = 67.7 \text{ km Mpc}^{-1}\text{s}^{-1}$) Ade et al. (2016). While this distance distribution ignores effects arising from the time-dependent star-formation rate, see Fishbach et al. (2018); You et al. (2020), it is satisfactory for our present purposes. By probing redshifts up to $z = 0.8$ (lookback time = 7 Gyr), it is in-principle possible to glean information about a time when the Universe was younger and the star formation rate was higher Madau & Dickinson (2014). In Fig. 2a and Fig. 2b we show the explicit redshift and luminosity distributions implied by our uniform-in-comoving volume source distribution with standard Λ CDM cosmology.

The final ingredient required to characterize our population of binary black holes is the duty cycle ξ , the fraction of segments containing a binary black hole signal. In the next section, we describe how the data are divided into 16 s segments. Current observations of binary black hole mergers suggest that two black holes merge somewhere in the Universe on average once every 223^{+352}_{-115} s. Most of these mergers probably take place at redshifts of $z < 2$ ($d_L \lesssim 15$ Gpc). Beyond $z = 2$, it is believed that star-formation rate decreases Madau & Dickinson (2014). With fewer stars, there are fewer black holes, and therefore fewer mergers. Assuming an average time between binary black hole of 100 s out to $d_L = 15$ Gpc, the duty cycle out to luminosity distances of 5 Gpc is approximately $\xi = 6.67 \times 10^{-3}$, and so we use this value for our injection study.

3 INFERENCES FROM THE GRAVITATIONAL-WAVE BACKGROUND

3.1 Overview

This section describes the statistical formalism that allows us to calculate the hyper-posterior distribution $p(\Lambda|\vec{d})$ for population parameters Λ described in Section 2 given some dataset \vec{d} . We follow the method described in Smith & Thrane (2018). The calculation is divided into the following steps.

- (i) We divide the data into 16 s segments. These segments are a convenient size so that any given segment is unlikely to contain more than one binary black hole signal. However, they are long enough that it is relatively unlikely for a binary black hole signal to fall on the boundary of two segments; see Smith & Thrane (2018).

Hyper parameter Λ_i	Description	Injection value
ξ	Astrophysical duty cycle	6.67×10^{-3}
$m_{\min}(M_\odot)$	Minimum black hole mass	$8.68 M_\odot$
$m_{\max}(M_\odot)$	Maximum mass of black holes in the power law component	$39.5 M_\odot$
$\mu_m(M_\odot)$	Mean of the Gaussian component of the primary mass distribution	$33.4 M_\odot$
σ_m	Standard deviation of the Gaussian component of the primary mass distribution	$1.08 M_\odot$
λ_m	Fraction of black holes in the Gaussian component of the primary mass distribution	0.340
α_m	Slope of the power law component of the primary mass distribution	2.00
β_m	Slope of the mass ratio distribution	-0.198
a_{\max}	Maximum spin magnitude	1.00
α_a	Spin-magnitude beta distribution slope parameter (rise)	1.50
β_a	Spin-magnitude beta distribution slope parameter (fall)	3.50
σ_{tilt}	Standard deviation of the spin-tilt angle distribution	1.00
ξ_{tilt}	Fraction of BBHs with Guassian distributed spin tilts	0.50

Table 1. Hyper parameters Λ_i of the binary black hole mass and spin population distributions.

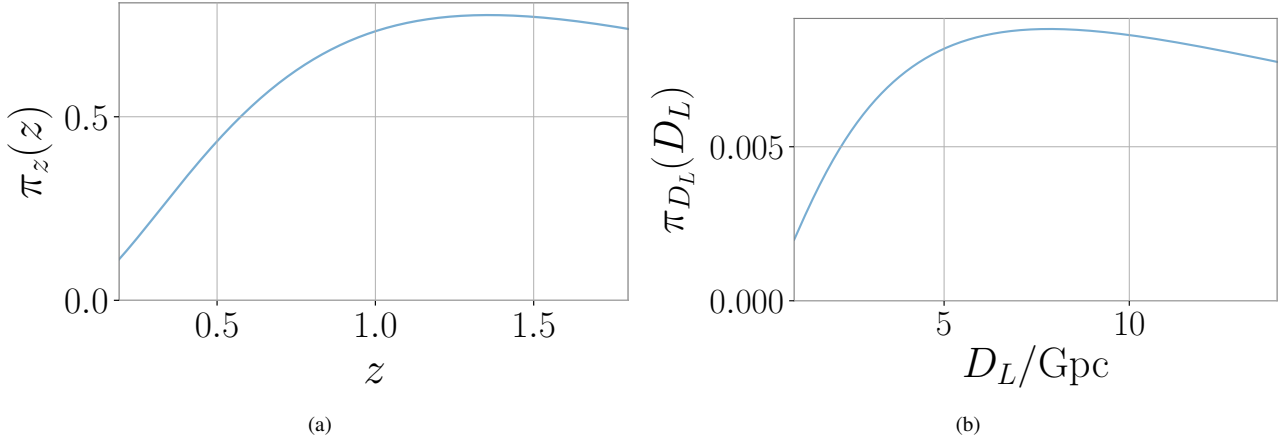


Figure 2. Prior distributions on redshift (left) and luminosity distance (right)

(ii) Run the nested sampling code **dynesty** Speagle (2020) (implemented in the **bilby** Ashton et al. (2018) Bayesian inference library) to generate posterior samples $\{\theta_{k,i}\}$ describing the mass and spins of individual binary black hole events in each segment. Additionally, **dynesty** estimates for each data segment, the noise evidence $\mathcal{Z}(d|\mathcal{H}_N)$ —that there is no binary black hole present—and “the default signal evidence” $\mathcal{Z}(d|\mathcal{H}_S)$ —that there is a binary black hole signal present given some default prior $\pi(\theta)$.

(iii) The posterior samples and evidences for each segments are used to define a “total likelihood”, defined in Eq. 1, which combines data from many segments. We discuss the hyper likelihood in greater detail in the next subsection.

(iv) Having defined the hyper likelihood, we use **dynesty** to generate hyper-posterior samples $\{\Lambda_i\}$, which provide a representation of $p(\Lambda|\vec{d})$.

Steps 1-2 are relatively straightforward. In the next subsection, we describe the hyper likelihood used in steps 3-4.

3.2 The hyper likelihood

Following Smith & Thrane (2018), we employ a likelihood function to describe the probability of some large dataset \vec{d} given a population of binary black hole described by hyper-parameters ξ (the fraction of data segments containing a signal) and Λ , which describes the

shape of the binary black hole mass and spin distributions

$$\mathcal{L}^{\text{tot}}(\vec{d}|\Lambda, \xi) = \prod_i^n \left[\xi \mathcal{L}(d_i|\Lambda, \mathcal{H}_S) + (1 - \xi) \mathcal{Z}(d_i|\mathcal{H}_N) \right]. \quad (1)$$

There is a lot to explain in this equation and the rest of this subsection is devoted to this task. The tot superscript denotes that this is the likelihood for the entire dataset \vec{d} . The expression includes a product over i data segments running from $i = 1$ to n . The term $\mathcal{L}(d_i|\Lambda, \mathcal{H}_S)$ is the single-segment Bayesian evidence for the data d_i in segment i given the signal hypothesis \mathcal{H}_S and hyper-parameters Λ . The term $\mathcal{Z}(d_i|\mathcal{H}_N)$ is the single-segment noise evidence for the data d_i in segment i . The hyper-parameter ξ is often referred to as “duty cycle,” and may be converted into a rate Smith & Thrane (2018).

The single-segment noise evidence $\mathcal{Z}(d_i|\mathcal{H}_N)$ is straightforwardly calculated for each segment using a Gaussian-noise likelihood³

$$\mathcal{Z}(d_i|\mathcal{H}_N) = \exp \left(-\frac{1}{2} \langle d_i, d_i \rangle \right). \quad (2)$$

³ We note that this is missing a normalisation factor, however, as this only depends on the PSD and not on the template, we can freely factor this out of the both the signal and noise evidences.

Here, we employ a noise-weighted inner product

$$\langle a, b \rangle \equiv 4\Re \Delta f \sum_k \frac{a^*(f_k)b(f_k)}{S_n(f_k)}, \quad (3)$$

where the sum is over frequency bins k with bin widths of Δf and $S_n(f)$ is the strain noise power spectral density.

The single-segment signal likelihood $\mathcal{L}(d_i|\Lambda, \mathcal{H}_S)$ is given by (Eq. 5) yielding:

$$\mathcal{L}(d_i|\Lambda, \mathcal{H}_S) \approx \frac{\mathcal{Z}(d_i|\mathcal{H}_S)}{n_s} \sum_{k=1}^{n_s} \frac{\pi(\theta_{k,i}|\Lambda)}{\pi(\theta_{k,i})}. \quad (4)$$

Here, $\mathcal{Z}(d|\mathcal{H}_S)$ is the Bayesian evidence for a binary black hole signal in segment i calculated using some default prior for the binary black hole parameters θ denoted $\pi(\theta)$. Assuming Gaussian noise, it is given by

$$\begin{aligned} \mathcal{Z}(d_i|\mathcal{H}_S) &\equiv \int d\theta_i \mathcal{L}(d_i|\theta, \mathcal{H}_S)\pi(\theta_i) \\ &= \int d\theta_i \exp\left(-\frac{1}{2}\langle d_i - h(\theta_i), d_i - h(\theta_i) \rangle\right) \\ &\quad \pi(\theta_i), \end{aligned} \quad (5)$$

where $h(\theta)$ is the gravitational waveform, in this case, calculated IMRPhenomPv2 approximant (Hannam et al. 2014); Smith et al. (2016). The integral in Eq. 5 is calculated numerically using the Bayesian inference library, bilby (Ashton et al. 2018) implementation of dynesty (Speagle 2020). In addition to calculating $\mathcal{Z}(d_i|\mathcal{H}_S)$, bilby outputs a list of n_s posterior samples $\{\theta_{k,i}\}$, which describe the posterior $p(\theta_i|d_i)$ given the default prior. It is sometimes said that the ratio of priors $\pi(\theta_{k,i}|\Lambda)/\pi(\theta_{k,i})$ in Eq. 4 serves to “reweight” the posterior samples calculated using the default prior $\pi(\theta)$ (Thrane & Talbot 2018).

3.3 The hyper-posterior

Using the hyper likelihood defined in Eq. 1, it is straightforward to obtain the (hyper-) posterior for duty cycle and the other hyper-parameters Λ

$$p(\Lambda, \xi|\vec{d}) = \frac{\mathcal{L}^{\text{tot}}(\vec{d}|\Lambda, \xi)\pi(\Lambda)\pi(\xi)}{\mathcal{Z}_{\Lambda}^{\text{pop}}}. \quad (6)$$

Here $\pi(\Lambda)$ is the hyper-parameter prior, which we take to be uniform for each hyper-parameter. The distribution $\pi(\xi)$ is the duty cycle prior. In a real analysis, one should choose a distribution, which uses a Poisson distribution to relate duty cycle to astrophysical rate; see Smith & Thrane (2018). However, for our present purposes, it is convenient to simply employ a uniform prior. The variable $\mathcal{Z}_{\Lambda}^{\text{pop}}$ is the hyper-evidence. They hyper-evidence can be used to carry out model selection between different population models; see Talbot & Thrane (2017b, 2018); Stevenson et al. (2015, 2017); Abbott et al. (2018a); Stevenson et al. (2017); Vitale et al. (2017); Talbot & Thrane (2017a); Gerosa & Berti (2017); Farr et al. (2017); Wysocki et al. (2018); Lower et al. (2018).

4 RESULTS: DEMONSTRATION WITH SIMULATED DATA

We analyze 5.5 days of simulated Advanced LIGO (aLIGO) design-sensitivity data (Aasi et al. 2015) containing an ensemble of 200 simulated binary black hole signals. We divide the data into 3×10^4

Parameter θ_i	Prior $\pi(\theta_i)$
m_1	Uniform($6M_{\odot}, 50M_{\odot}$)
q	Uniform(0,2,1)
D_C^3	Uniform($1\text{Gpc}^3, 5^3\text{Gpc}^3$)
t_c	Uniform(0s, 16s)
$\cos i$	Uniform(-1,1)
ϕ_c	Uniform(0, 2π)
ψ	Uniform(0, π)
$\cos t_1$	Uniform(-1,1)
$\cos t_2$	Uniform(-1,1)
ϕ_{12}	Uniform(0, 2π)
ϕ_{JL}	Uniform(0, 2π)
a_1	Uniform(0,1)
a_2	Uniform(0,1)
α	Uniform(0, 2π)
$\cos \delta$	Uniform(-1,1)

Table 2. Priors on the 15 binary black hole signal parameters, $\pi(\theta)$. The priors are used in Stage 1 of the hierarchical population inference (Sec. 3). The parameters are the source-frame primary black-hole mass, m_1 ; mass ratio q ; co-moving distance D_C ; time of coalescence t_c ; cosine of the orbital inclination $\cos i$; phase at coalescence ϕ_c ; polarization phase ψ ; cosine of the spin-tilt angles $\cos t_1$ and $\cos t_2$; the angle between the two spin vectors ϕ_{12} ; angle between the total and orbital angular momentum ϕ_{JL} ; dimensionless spin magnitudes a_1 and a_2 ; right ascension α ; and cosine of the declination δ .

sixteen-second segments. This yields a duty cycle $\xi = 200/30000 = 6.67 \times 10^{-3}$. We derive the duty cycle by first assuming an average merger range of binary black holes of 1 per 100s. We then assume that the merger rate drops significantly beyond a redshift of $z \sim 2$ so that their contribution can be effectively ignored. The fraction of all binaries contained in the volume with maximum redshift considered here, $z = 0.8$, is approximately 4%. The average merger rate out to $z = 0.8$ is then approximately one merger per 45min. In 5.5 days this yields 176 binary mergers, however we choose to round up to 200.

The masses and spins of the binary black hole’s are drawn from the mass and spin distributions described in Sec. 2. The remaining “extrinsic” parameters are drawn using standard distributions. All of the signals in our injection set are below the usual threshold for matched-filter network SNR: $\rho_{\text{network}}^{\text{th}} = 12$. Based on results from Smith & Thrane (2018), we expect the binary black hole background to be detectable with approximately one day of aLIGO design sensitivity data.

We estimate the signal and noise evidence \mathcal{Z}_S , \mathcal{Z}_N , and obtain posterior samples for binary black hole source parameters for every data segment. The priors, summarized in Table 2, and are chosen to be relatively uninformative so we can recycle the posterior samples later. We then use the sets of evidence and posterior samples as input to Eq. 3.3 to compute the posterior for Λ —the population mass and spin distribution parameters—and ξ , the astrophysical duty cycle.

The computational cost of running full parameter estimation on 3×10^4 16-second data segments is kept manageable by explicitly marginalizing over three parameters, which are difficult to sample: comoving distance, coalescence time, and coalescence phase; see e.g., Thrane & Talbot (2018) for the details of these marginalization schemes. By marginalizing over these parameters, we significantly decrease the convergence time, and hence run time, of computing evidences and drawing posterior samples in step 1.

We find that the background is detectable within one week out to comoving distances of 5 Gpc, assuming masses and spins drawn

from the distribution described in Sec. 2. The posterior distribution on ξ is consistent with the true value of $\xi = 0.67\%$, and the log Bayes factor (Eq. 15 of Smith & Thrane (2018)) overwhelmingly supports a detection of a population of compact binaries: $\ln \text{BF} \approx 700$, confirming the previous result from Smith & Thrane (2018) with a different, more realistic population of BBH.

We find that we can begin to constrain some of the mass and spin population parameters using the 200 unresolved mergers in our simulated data. In Fig. 3a we show posterior predictive distributions for different mass and spin parameters. The posterior predictive distributions reflect our updated prior based on information from our hyper-posteriors; see Thrane & Talbot (2018). The contours represent the $1 - \sigma$ and $2 - \sigma$ credible intervals.

In Fig. A1, we show posterior distributions for hyper-parameters associated with the duty cycle and mass parameters. In A2, we show posterior distributions for the parameters associated with the Gaussian component of the mass population model. In Fig. A3, we show posterior distributions for hyper-parameters describing black hole spins.

5 HOW SENSITIVE ARE WE TO SUBTHRESHOLD EVENTS?

In this section, we investigate where the information for our analysis comes from. Is our resolving power coming primarily from binaries just below the detection threshold, or do we gain information from weaker events as well? To address this question, we carry out a follow-up study where we introduce a new hyper-parameter, d_{\max} , the maximum comoving distance for binary mergers. In our new population model, the rate of binary mergers drops to zero for distances greater than d_{\max} . The d_{\max} parameter is not physical, but it is useful for our present investigation: if the data disfavor some value of d_{\max} (less than the true value of d_{\max}), then we are getting information from that distance. We set the true value of $d_{\max} = 5100$ Gpc (comoving distance) and then use hierarchical inference to obtain a posterior for d_{\max} . We calculate the posterior on d_{\max} for different Gaussian mass distributions with standard deviation $\sigma = 0.3 M_{\odot}$ and means $\mu = (5M_{\odot}, 10M_{\odot}, 20M_{\odot}, 30M_{\odot})$. The results are shown in Fig. 4.

The posterior on d_{\max} peaks at the true value of $d_{\max} = 5100$ Mpc (comoving distance). The d_{\max} likelihood is clearly informative for distances greater than the distance of the furthest $\text{SNR} > 12$ event, which is marked by the horizontal solid black line in Fig. 4. This is true for all masses considered in our study. A similar conclusion is made for the most distant event with $\text{SNR} > 10$,

marked by the horizontal dashed line and the most distant event with $\text{SNR} > 8$, marked the horizontal dotted line. (No events with $\text{SNR} > 12$ were used to obtain this hyper-posterior.) This plot is a good indication that we are indeed getting information from sub-threshold events.

6 CONCLUSIONS

Our results demonstrate that the astrophysical gravitational-wave background can be used to constrain the population properties of binary black holes together with “gold plated” foreground signals. By applying hierarchical inference to all available data—irrespective of whether it contains a gravitational-wave signal or not—we eliminate selection bias. By carrying out population inferences with sub-threshold events we help extend the reach of the current generation of observatories to greater distances. A crucial next step is the demonstration of the algorithm using real data. A mock data challenge is underway to show how the algorithm performs in realistic conditions. Another goal is to determine how much information can be inferred about the redshift dependence of binary-black hole mass and spin properties.

7 ACKNOWLEDGEMENTS

RS, CT, FHV, and ET are supported by the Australian Research Council (ARC) CE170100004. ET is supported by ARC FT150100281. We thank Stuart Anderson and the LIGO Data Grid for assistance with computing infrastructure, and Maya Fishbach, Thomas Callister and Thomas Dent for helpful comments and suggestions. We acknowledge the OzStar cluster for providing graphical processor units to carry out some of our calculations.

APPENDIX A: POPULATION HYPER PARAMETER ESTIMATION

The one and two dimensional PDFs for the population hyper parameters used in this study are shown below.

APPENDIX B: POPULATION MODEL DETAILS

B1 Source-frame mass

The conditional prior for binary black hole mass is:

$$\pi_m(m_1|\Lambda) = \left[(1 - \lambda_m)A(\Lambda) m_1^{-\alpha} \Theta(m_{\max} - m_1) + \lambda_m B(\Lambda) \exp\left(-\frac{(m_1 - \mu_m)^2}{2\sigma_m^2}\right) \right] S(m_1|m_{\min}, \delta m),$$

$$\pi_q(q|m_1, \Lambda) = C(m_1, \Lambda) q^{\beta} S(m_2|m_{\min}, \delta m).$$
(B1)

The first equation describes the prior probability of the primary mass m_1 (corresponding to the heavier of the two black holes in a binary black hole) given the hyper-parameters Λ . The second equation describes the prior probability of the mass ratio $q = m_2/m_1$ given m_1 and Λ .

The fraction of black holes in the Gaussian component is λ_m .

The distribution of mass ratios follows a power-law distribution with unknown spectral index β . Additionally, there is a smoothing parameter δ_m which enables the distribution to have a smooth turn-on at low masses.

The prior for primary mass $\pi(m_1|\Lambda)$ is constructed from two

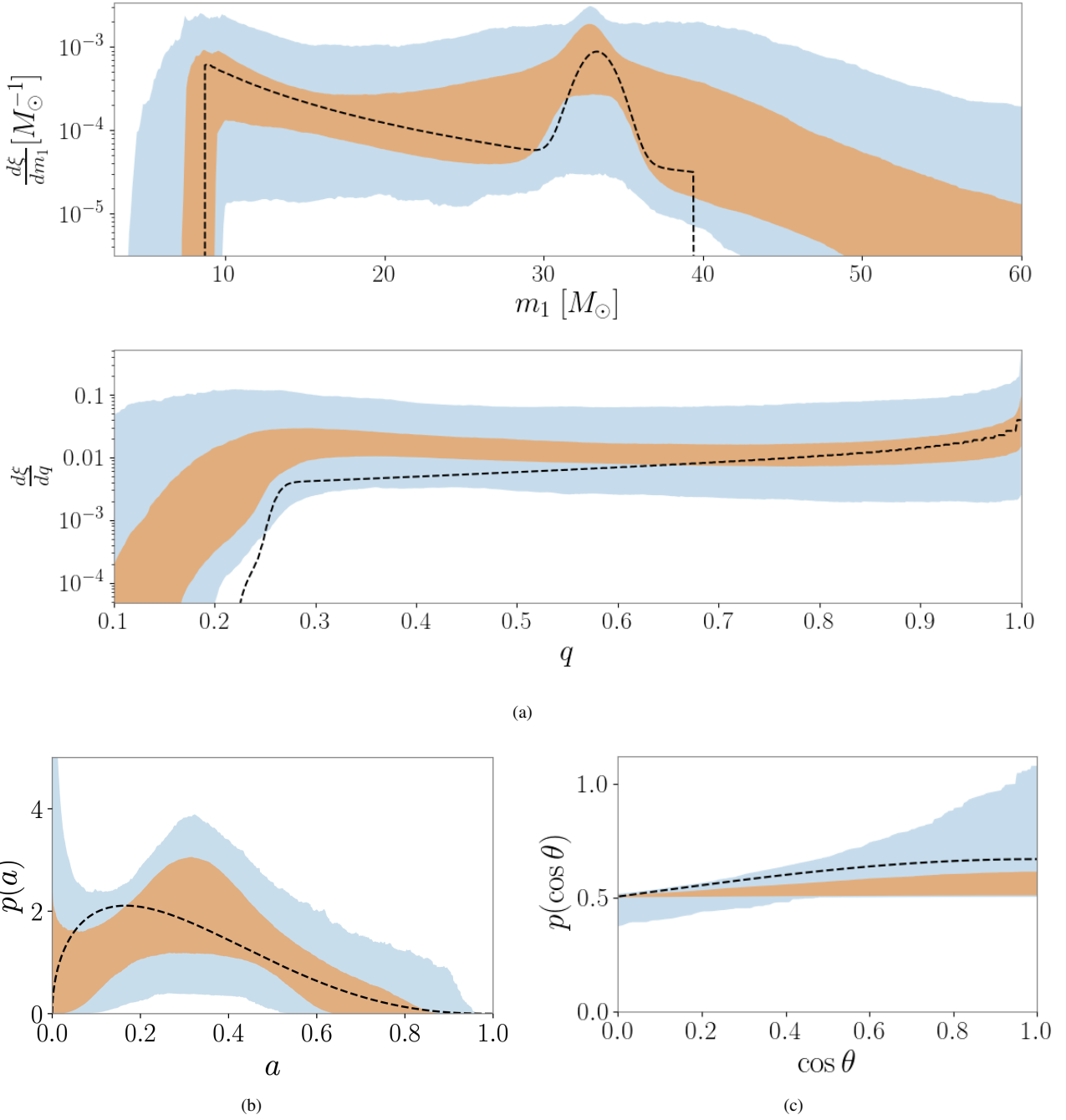


Figure 3. Posterior predictive distributions of binary black hole parameters. These results are obtained using five and a half days of simulated aLIGO data containing 395 binary black holes signals. The dashed line is the true distribution, while the red contours represent the 50% (light) and 90% credible intervals on the inferred distributions. The parameters are: (top) primary black hole mass m_1 , (center) mass ratio q , (lower left) spin magnitude a , (lower right) cosine spin tilt $\cos \theta$.

pieces. The first term

$$(1 - \lambda_m) A(\Lambda) m_1^{-\alpha} \Theta(m_{\max} - m_1), \quad (\text{B2})$$

describes a power-law distribution with index $\alpha \in \Lambda$. The Heaviside step-function cuts off the distribution at $m_{\max} \in \Lambda$. One minus the term $\lambda_m \in \Lambda$ is the fraction of events that are part of this power-law distribution. The term $A(\Lambda)$ is a normalization constant. This term is motivated by the fact that the stellar mass function is power-law distributed as well as evidence of a cut-off in the black hole mass

spectrum Fishbach et al. (2017); Talbot & Thrane (2017b); Abbott et al. (2018a).

The second term in $\pi(m_1 | \Lambda)$

$$\lambda_m B(\Lambda) \exp \left(-\frac{(m_1 - \mu_m)^2}{2\sigma_m^2} \right), \quad (\text{B3})$$

corresponds to a Gaussian distribution with mean $\mu_m \in \Lambda$ and width $\sigma_m \in \Lambda$. The fraction of events that are part of the Gaussian distribution is given by λ_m . The $B(\Lambda)$ term is a normalization constant.

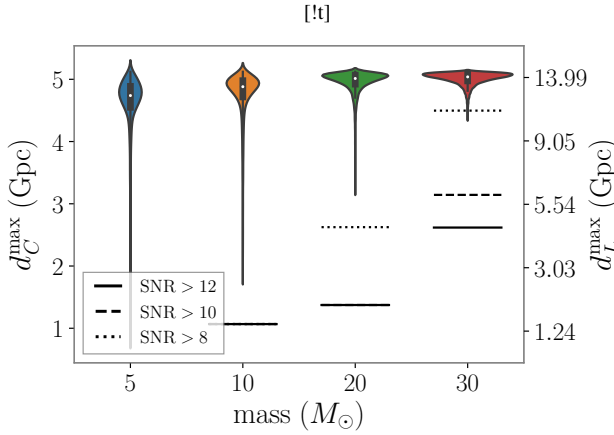


Figure 4. Violin plots of the comoving and luminosity d_{\max} posterior obtained by running hierarchical inference with different mass distributions. Each distribution is set to be Gaussian with standard deviation $\sigma = 0.3M_{\odot}$ and means $\mu = (5, 10, 20, 30) M_{\odot}$. The horizontal solid, dashed and dotted lines correspond to the most distant event observed with network SNR>12, SNR>10 and SNR>8 for each mass respectively. The posteriors peak at the true value $d_{\max} = 5100$ Mpc (comoving distance) and the most distant events with SNR> 12 lie below the d_{\max} posteriors, suggesting that we obtain most of the information from subthreshold events.

This term is motivated by the possibility of a bump in the black hole mass spectrum from pulsational pair instability supernovae [Talbot & Thrane \(2018\)](#); [Abbott et al. \(2018a\)](#); [Marchant, Renzo, Farmer, Pappas, Taam, de Mink & Kalogera \(Marchant et al.\)](#).

To the far right of the expression for $\pi(m_1|\Lambda)$ is a third term

$$\begin{aligned} S(m, m_{\min}, \delta m) &= (\exp f(m - m_{\min}, \delta m) + 1)^{-1} \\ f(m, \delta m) &= \frac{\delta m}{m} - \frac{\delta m}{m - \delta m}. \end{aligned} \quad (\text{B4})$$

The m_{\min} parameter enforces a minimum black hole mass and δm is the mass range over which the black hole mass spectrum falls to zero. This term is motivated by the fact that there is likely a minimum black hole mass, at least for black holes made through stellar collapse [Talbot & Thrane \(2018\)](#).

The conditional prior for mass ratio is described by a power law with index $\beta \in \Lambda$. The smoothing function S applies a low-mass cut-off in the secondary mass m_2 , again using minimum mass m_{\min} and δm for the mass range over which the mass spectrum falls to zero. The variable $C(m_1, \Lambda)$ is a normalization constant.

B2 Lab-frame mass

The binary black hole lab-frame mass is a function of redshift because

$$m_l = (1+z)m_s, \quad (\text{B5})$$

where m_s is the source-frame mass and m_l is the lab-frame mass. When considering events at cosmological distances, the prior distributions for lab-frame masses become covariant with luminosity distance D_L due to cosmological redshift. In the source frame, the distributions of black hole mass and redshift are separable so that

$$\pi(m_s, z) = \pi_m(m_s)\pi_z(z) \quad (\text{B6})$$

Whatever form the distributions we choose for $\pi_z(z)$ and $\pi_m(m_s)$,

they imply some prior for the lab-frame mass:

$$\begin{aligned} \pi(z, m_l) &= \pi(z, m_s(m_l)) \left| \frac{dm_s}{dm_l} \right| \\ &= (1+z)^{-1} \pi(z, m_l/(1+z)). \end{aligned} \quad (\text{B7})$$

B3 Spin

The distribution of spin magnitudes (a_1, a_2) are assumed to each follow a beta distribution described by three parameters $(\alpha_a, \beta_a, a_{\max}) \in \Lambda$. By treating a_{\max} as a free parameter, our model is a generalization of the prescription from [Wysocki et al. \(2018\)](#). The conditional prior for spin magnitude is

$$\pi_a(a|\alpha_a, \beta_a, a_{\max}) = \frac{a^{(\alpha_a-1)}(a_{\max}-a)^{(\beta_a-1)}}{a_{\max}^{(\alpha_a+\beta_a-1)} B(\alpha_a, \beta_a)}. \quad (\text{B8})$$

Here $B(\alpha_a, \beta_a)$ is the Beta function.

We characterize the black hole spin orientation in terms of the cosine of the polar angle between the orbital angular momentum and the black hole spin $z_{1,2} \equiv \cos(t_{1,2})$ where $t_{1,2}$ is the polar angle. We ignore the azimuthal angle, which has a comparatively small effect on the gravitational waveform. We assume that the distribution of spin orientations is a mixture of an isotropic component and a preferentially aligned component modeled as a truncated half-Gaussian with unknown width σ_{tilt} and which peaks at $t_1 = t_2 = 1$.

$$\begin{aligned} \pi(z_1, z_2 | \sigma_{\text{tilt}}, \lambda_{\text{tilt}}) &= \frac{(1-\lambda_{\text{tilt}})}{4} \\ &+ \frac{\lambda_{\text{tilt}}}{2\pi} \prod_{i \in \{1,2\}} \frac{e^{-(1-z_i)^2/(2\sigma_{\text{tilt}}^2)}}{\sigma_{\text{tilt}} \operatorname{erf}(\sqrt{2}/\sigma_{\text{tilt}})}. \end{aligned} \quad (\text{B9})$$

The isotropic distribution is a model for mergers in dense stellar environments such as globular clusters, where spin orientations are expected to be isotropically oriented. The aligned distribution models binaries formed in the field. The fraction of binaries in the preferentially aligned component is ξ_{χ} . We assume that both component spins are independently drawn from the same distribution.

REFERENCES

- Aasi J., et al., 2015, *Class. Quant. Grav.*, 32, 074001
- Abbott B. P., et al., 2016a, *Phys. Rev. X*, 6, 041015
- Abbott B. P., et al., 2016b, *Phys. Rev. Lett.*, 116, 131102
- Abbott B. P., et al., 2018a, *Phys. Rev. Lett.*, 120, 091101
- Abbott B. P., et al., 2018b, *Phys. Rev. Lett.*, 121, 161101
- Abbott B. P., et al., 2019, *Phys. Rev. X*, 9, 031040
- Abbott B. P., et al., 2018a
- Abbott B. P., et al., 2018b
- Acernese F., et al., 2014, *Classical and Quantum Gravity*, 32, 024001
- Ade P. A. R., et al., 2016, *Astronomy & Astrophysics*, 594, A13
- Akutsu T., et al., 2019, *Nature Astronomy*, 3, 354–360
- Ashton G., et al., 2018
- Farr W. M., Stevenson S., Miller M. C., Mandel I., Farr B., Vecchio A., 2017, *Nature*, 548, 426
- Fishbach M., Holz D. E., 2017, *Astrophys. J. Lett.*, 851, L25
- Fishbach M., Holz D., Farr B., 2017, *Astrophys. J. Lett.*, 840, L24
- Fishbach M., Holz D. E., Farr W. M., 2018, *Astrophys. J. Lett.*, 863, L41
- Gaebel S. M., Veitch J., Dent T., Farr W. M., 2018
- Gerosa D., Berti E., 2017, *Phys. Rev. D*, 95, 124046
- Hannam M., Schmidt P., Bohé A., Haegel L., Husa S., Ohme F., Pratten G., Pürrer M., 2014, *Phys. Rev. Lett.*, 113, 151101

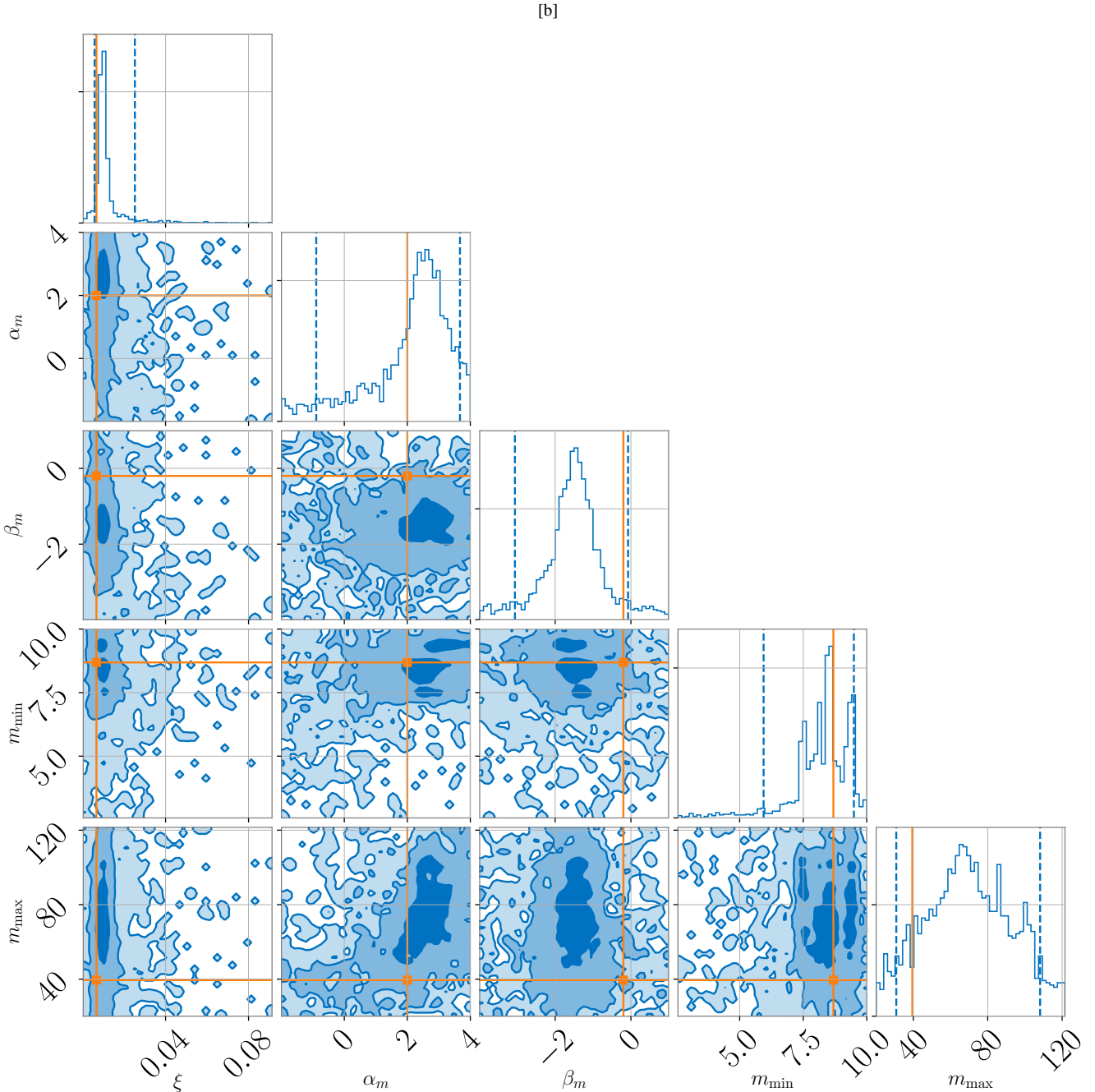


Figure A1. One- and two-dimensional (hyper-) posterior distribution. This figure showcases duty cycle ξ and hyper-parameters related to the mass-spectrum peak. From left to right; the astrophysical duty cycle ξ ; the slope of the power law component of the primary mass distribution α_m ; the slope of the mass ratio distribution β_m ; the minimum black hole mass m_{\min} ; and the maximum black hole mass in the power-law component m_{\max} . The dashed lines are the 90% credible intervals.

- Hernandez-Vivanco F., Smith R. J. E., Thrane E., Lasky P. D., 2019, Phys. Rev. D, 100, 043023
 Lower M. E., Thrane E., Lasky P. D., Smith R., 2018, Phys. Rev. D, 98, 083028
 Madau P., Dickinson M., 2014, [Annual Review of Astronomy and Astrophysics](#), 52, 415
 Maggiore M., 2000, Phys. Rep., 331, 283
 Mandel I., Farr W. M., Gair J. R., 2018
 Marchant P., Renzo M., Farmer R., Pappas K. M. W., Taam R. E., de Mink S., Kalogera V., Ng K. K. Y., Vitale S., Zimmerman A., Chatzioannou K., Gerosa D., Haster

- C.-J., 2018, Phys. Rev. D, 98, 083007
 Raidal M., Vaskonen V., Veermäe H., 2017, Journal of Cosmology and Astroparticle Physics, 2017, 037
 Smith R., Thrane E., 2018, Phys. Rev. X, 8, 021019
 Smith R., Field S. E., Blackburn K., Haster C.-J., Pürrer M., Raymond V., Schmidt P., 2016, Phys. Rev. D, 94, 44031
 Speagle J. S., 2020, [Monthly Notices of the Royal Astronomical Society](#), 493, 3132–3158
 Stevenson S., Ohme F., Fairhurst S., 2015, [Astrophys. J.](#), 810, 58
 Stevenson S., Berry C., Mandel I., 2017, MNRAS, 471, 2801
 Talbot C., Thrane E., 2017a, Phys. Rev. D, 96, 023012

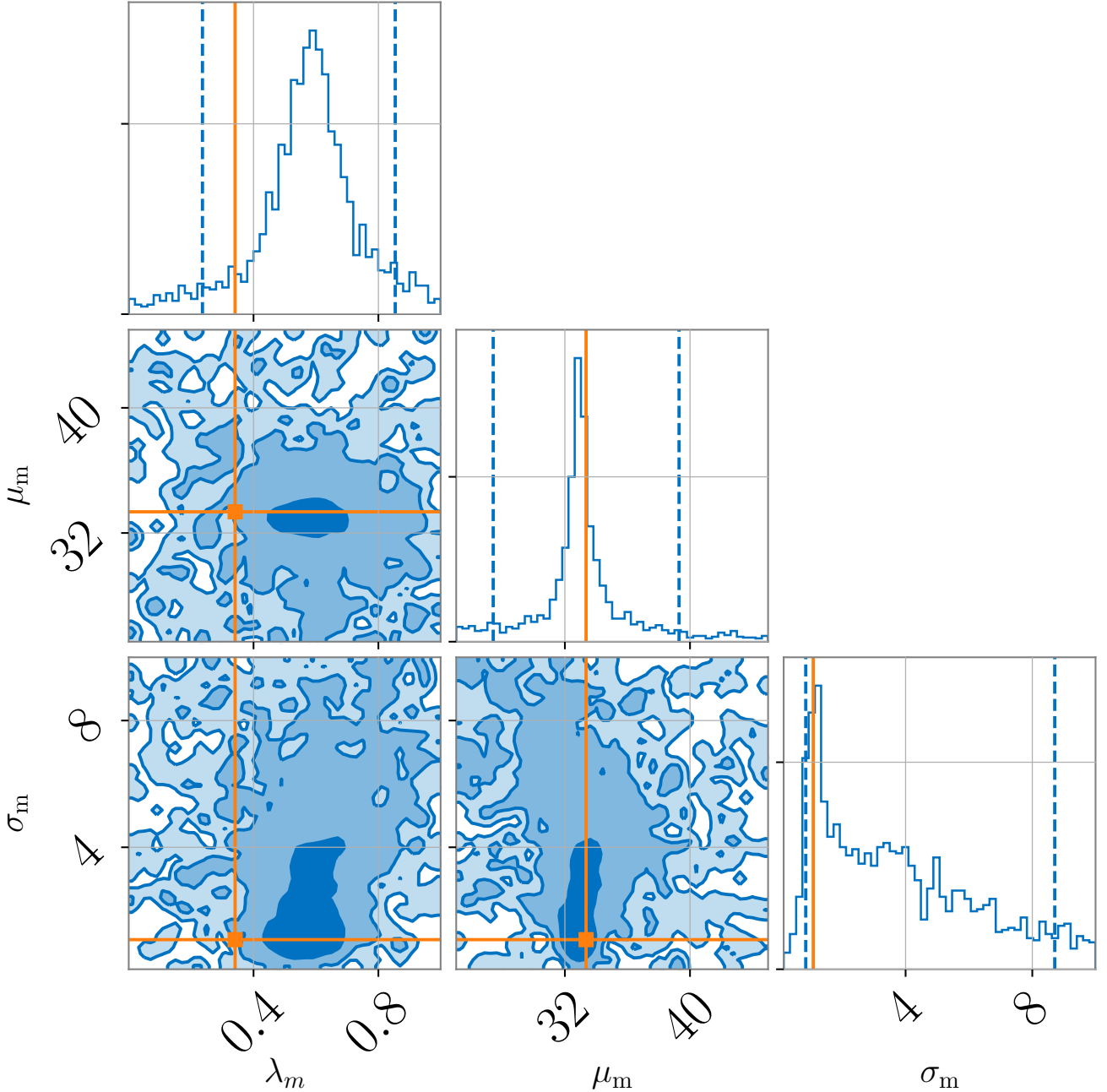


Figure A2. One- and two-dimensional (hyper-) posterior distributions. This figure showcases duty cycle hyper-parameters related to shape of the binary black hole mass spectrum. From left to right: The fraction of black holes in the Gaussian component of the primary mass distribution λ_m ; the mean of the Gaussian component of the primary mass distribution μ_m ; and the standard deviation of the Gaussian component of the primary mass distribution σ_m . The dashed lines are the 90% credible intervals.

Talbot C., Thrane E., 2017b, *Phys. Rev. D*, 96, 023012
 Talbot C., Thrane E., 2018, *The Astrophysical Journal*, 856, 173
 Thrane E., Talbot C., 2018
 Tiwari V., Fairhurst S., Hannam M., 2018, *Astrophys. J.*, 868, 140

Vitale S., Lynch R., Sturani R., Graff P., 2017, *Class. Quant. Grav.*, 34, 03LT01
 Wysocki D., Lange J., O.'shaughnessy R., 2018
 You Z.-Q., Zhu X.-J., Ashton G., Thrane E., Zhu Z.-H., 2020

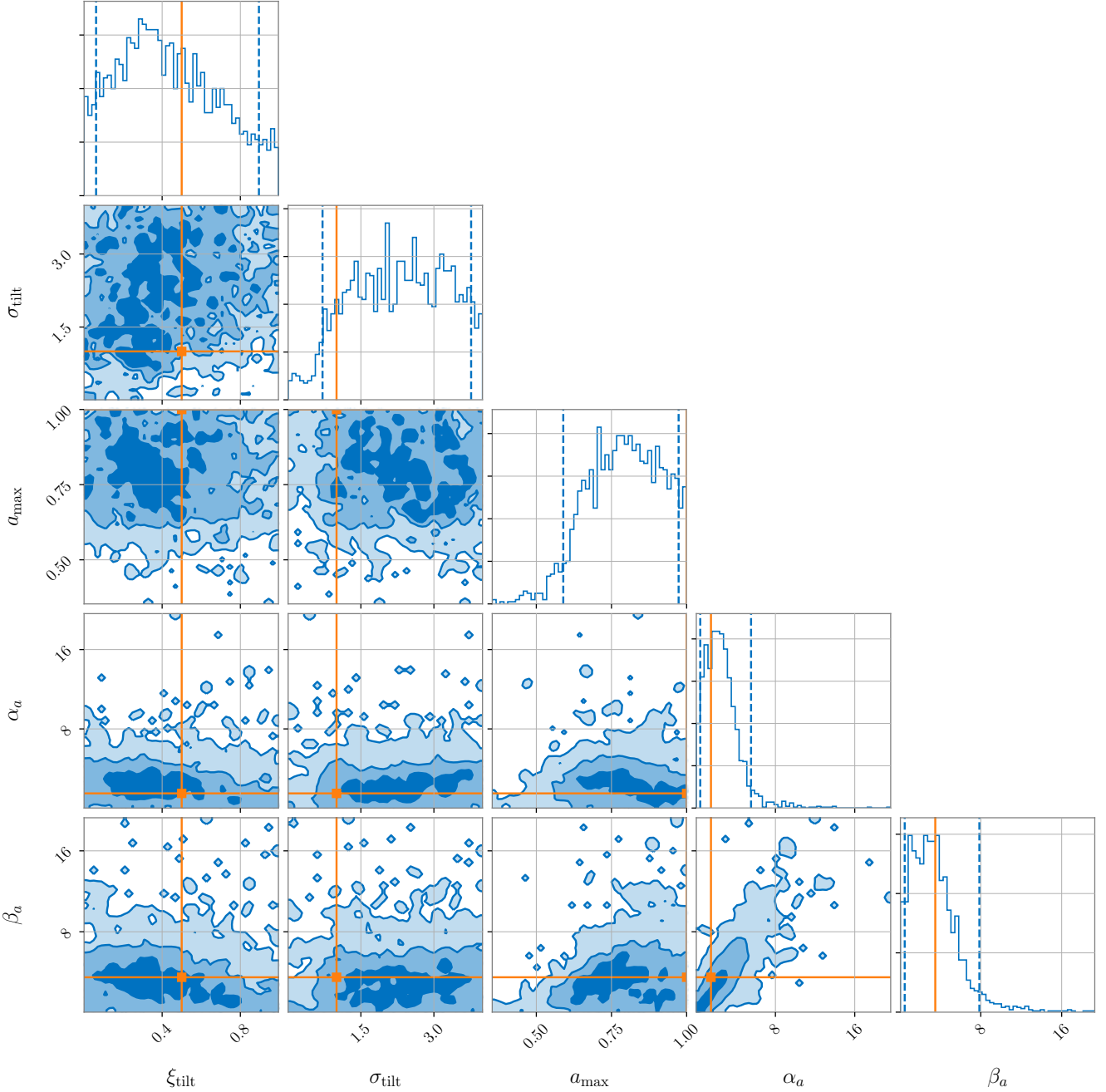


Figure A3. One- and two-dimensional (hyper-) posterior distributions. This figure shows hyper-parameters related to the distribution of black hole spins. From left to right: the fraction of BBHs with Gaussian distributed spin tilts ξ_{tilt} ; the standard deviation of the spin-tilt angle distribution σ_{tilt} ; the maximum spin magnitude a_{max} ; the spin-magnitude beta distribution slope parameter (rise) α_a ; and the spin-magnitude beta distribution slope parameter (fall) β_a . The dashed lines are the 90% credible intervals.